Chapter 2
Two-Photon Interference

2.1 Classical Interferometry

Interferometry using various portions of the electromagnetic spectrum has a long history, extending back to the beginning of the nineteenth century in the optical case, and expanding far into other parts of the electromagnetic spectrum by the mid-twentieth century. During this time, interferometry has been used both as a probe for investigating the properties of light itself and as a practical tool for making high-precision measurements of other objects and phenomena. The applications range from measurement of lattice structures in solids and determination of stellar diameters to searches for gravity waves, a luminiferous ether, and extra space-time dimensions.

The archetypal interference experiment is the Young double slit experiment (Fig. 2.1), in which a wavefront is split into two components. In general, each component travels a slightly different distance as they make their way to a given point of the viewing screen. The two recombined wavefronts thus have different phase values due to their different propagation distances, with the result that bright and dark regions are formed on the screen from the corresponding constructive and destructive interference.

When the double slit experiment is examined at the level of individual photons, it is tempting to think of one photon passing through the top slit and the other passing through the bottom slit, followed by interference of one photon with the other at the final screen. However, this cannot be the case. To see this, suppose that a photographic plate is placed at the screen location to record photon arrival events. Experimentally, even if the intensity is reduced to the point where there is negligible probability of more than one photon reaching the slits at a given time, interference still arises (see [1], Sect. 1.1). Rather, each photon has two paths that can be followed to reach the same point on the screen, one path through each slit. If there is no way to determine which path was taken, then the superposition principle tells us that the amplitudes for both paths must be added; what interferes then are these two amplitudes for

D.S. Simon et al., *Quantum Metrology, Imaging, and Communication*,
Quantum Science and Technology, DOI 10.1007/978-3-319-46551-7_2

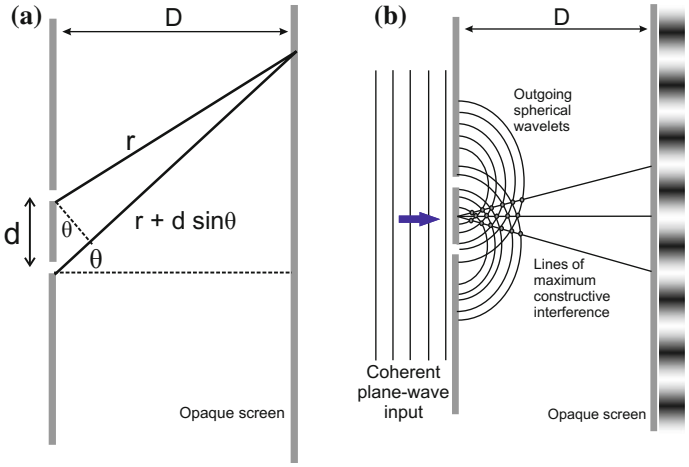

Fig. 2.1 Young double-slit interference. **a** The beams from the two slits travel slightly different distances to reach a point on the screen, resulting in a relative phase shift between the beams, causing *bright* and *dark bands*, **b** the regions of constructive and destructive interference, constructive interference occurring at angles θ such that the phase difference $\frac{d \sin\theta}{\lambda}$ is an integer multiple of 2π

different behaviors of the *same* photon. Turning up the intensity, all interference arising in classical optics can be viewed as interference of light with itself in this manner. In the case both of single photon interference and of high-intensity classical interference, this situation is captured by the definition of first-order correlation $g^{(1)}$ given in the next section. For such interference to arise, it is necessary for the different intermediate histories of the photons to be indistinguishable with respect to the experimental apparatus: if there is any way to determine which history is followed, then the interference pattern becomes washed out (see [1], Sect. 3.6, [2]).

A more versatile way to produce interference for many applications is through the use of interferometers, such as the Mach–Zehnder and Hong–Ou–Mandel interferometers in the case of spatial interference. When combined with entangled two-photon sources like spontaneous parametric down conversion discussed, these open up a number of new possibilities, including true multi-photon interference of a kind that does not occur in classical interferometry. In these processes, different potential histories of the same multi-photon set interfere. In order to quantify the non-classical nature of these interference effects, we must define a new type of correlation function, the second-order correlation function $g^{(2)}$.

The first and second-order correlation functions are introduced in the next section, with a more detailed discussion of interferometers in the following sections.

2.2 Correlation Functions

2.2.1 First-Order Correlations

We wish to be able to compare the field amplitude at one space-time point (position $\boldsymbol{x}_1$, time t_1) to the field at a different point ($\boldsymbol{x}_2$, t_2). Young two-slit interference corresponds to a special case where $\boldsymbol{x}_1 = \boldsymbol{x}_2$ and $t_1 = t_2$; in other words, the two fields were directed to the same point before measuring the combined intensity.

To compare fields at different points, we define the *first-order correlation function* or *amplitude correlation function* [3],

$$G^{(1)}(\boldsymbol{r}_1, \boldsymbol{r}_2; t_1, t_2) = \langle \hat{E}^{(-)}(\boldsymbol{r}_1, t_1) E^{(+)}(\boldsymbol{r}_2, t_2) \rangle, \tag{2.1}$$

where $\langle \ldots \rangle$ denotes the quantum expectation value in the relevant state and $\hat{E}^{(\pm)}$ are the positive and negative frequency parts of the electric field operator (see "Appendix B"). This function obeys

$$G^{(1)}(\boldsymbol{r}_1, \boldsymbol{r}_2; t_1, t_2) = \left(G^{(1)}(\boldsymbol{r}_2, \boldsymbol{r}_1; t_2, t_1)\right)^* \tag{2.2}$$

$$G^{(1)}(\boldsymbol{r}, \boldsymbol{r}; t, t) \geq 0, \tag{2.3}$$

$$\left|G^{(1)}(\boldsymbol{r}_1, \boldsymbol{r}_2; t_1, t_2)\right|^2 \leq G^{(1)}(\boldsymbol{r}_1, \boldsymbol{r}_1; t_1, t_1) G^{(1)}(\boldsymbol{r}_2, \boldsymbol{r}_2; t_2, t_2). \tag{2.4}$$

The normalized correlation function

$$g^{(1)}(\boldsymbol{r}_1, \boldsymbol{r}_2; t_1, t_2) = \frac{G^{(1)}(\boldsymbol{r}_1, \boldsymbol{r}_2; t_1, t_2)}{\left[G^{(1)}(\boldsymbol{r}_1, \boldsymbol{r}_1; t_1, t_1) G^{(1)}(\boldsymbol{r}_2, \boldsymbol{r}_2; t_2, t_2)\right]^{1/2}} \tag{2.5}$$

$$= \frac{\langle \hat{E}^{(-)}(\boldsymbol{r}_1, t_1) E^{(+)}(\boldsymbol{r}_2, t_2) \rangle}{\sqrt{\langle \hat{E}^{(-)}(\boldsymbol{r}_1, t_1) E^{(+)}(\boldsymbol{r}_1, t_1) \rangle \langle \hat{E}^{(-)}(\boldsymbol{r}_2, t_2) E^{(+)}(\boldsymbol{r}_2, t_2) \rangle}}, \tag{2.6}$$

therefore, satisfies $0 \leq g^{(1)}(\boldsymbol{r}_1, \boldsymbol{r}_2; t_1, t_2) \leq 1$. Optical correlation functions are also sometimes called *coherence functions* and the absolute value $|g^{(1)}(\boldsymbol{r}_1, \boldsymbol{r}_2; t_1, t_2)|$ is called the *degree of coherence*.

Setting the two positions equal to each other gives the temporal correlation function,

$$g^{(1)}(\tau) = \frac{G^{(1)}(\boldsymbol{r}, \boldsymbol{r}; t, t+\tau)}{G^{(1)}(\boldsymbol{r}, \boldsymbol{r}; t, t)} = \frac{G^{(1)}(\boldsymbol{r}, \boldsymbol{r}; 0, \tau)}{G^{(1)}(\boldsymbol{r}, \boldsymbol{r}; 0, 0)}. \tag{2.7}$$

Here, we have assumed that the fields are stationary, i.e. that their correlations depend only on coordinate differences $\Delta\boldsymbol{r} = \boldsymbol{r}_2 - \boldsymbol{r}_2$ and $\tau = t_2 - t_1$, not on the individual values $\boldsymbol{r}_1$, $\boldsymbol{r}_2$, t_1, and t_2 themselves. It is clear that $g^{(1)}(0) = 1$. Except for the case of perfect coherence (see below), the temporal coherence function decays at long times: $g^{(1)}(\tau) \to 0$ as $\tau \to \infty$.

A thermal light source consists of many atoms, usually in the form of a gas, radiating independently. Collisions between the atoms cause random phase jumps in the emitted radiation, so that the light emitted remains coherent only over short time periods determined by the mean time between collisions. In addition, the light may scatter multiple times before leaving the source, adding further randomness to the phases. For a quasi-monochromatic field of the form (suppressing the spatial dependence for simplicity) $\hat{E}^{(-)}(t) = E_0\ e^{-i\omega t} e^{i\phi(t)}\ \hat{a}$, the temporal correlation function has the form

$$g^{(1)}(\tau) = e^{-i\omega\tau} \langle e^{\phi(t+\tau)-\phi(t)} \rangle. \tag{2.8}$$

The first exponential factor provides a rapid oscillation, while the expectation value provides a much more slowly varying envelope, so that $g^{(1)}(\tau)$ generally has an overall form as in Fig. 2.2. The time at which the correlation begins rapidly decreasing in amplitude is called the *coherence time*, τ_c. The coherence time is generally inversely proportional to the bandwidth $\Delta\omega$ of the light.

Light can be classified by its coherence properties. If the light is perfectly monochromatic ($\Delta\omega = 0$), then it is called *perfectly coherent* or simply *coherent*, with coherence time $\tau_c = \infty$. A laser is often considered to be a good approximation to a coherent light source, with a narrow bandwidth and a long coherence time. On the other hand, if $\tau_c = 0$ (and therefore $\Delta\omega = \infty$), the light is *incoherent*. For

(a)

Temporal coherence	τ_c	$\Delta\omega$	$g^{(1)}(\tau)$
Perfectly coherent	$\tau_c \to \infty$	$\Delta\omega \to 0$	$g^{(1)}(\tau) \sim$ constant
Partially coherent	τ_c finite	$\Delta\omega$ finite	$g^{(1)}(\tau) \sim e^{-(\lvert\tau\rvert/\tau_c)^\alpha}$
Perfectly incoherent	$\tau_c \to 0$	$\Delta\omega \to \infty$	$g^{(1)}(\tau) \sim \delta(\tau)$

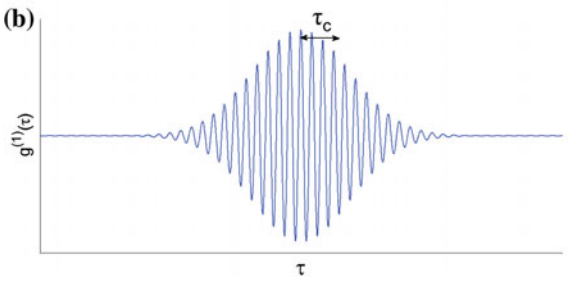

Fig. 2.2 **a** The possible types of first-order coherence. In the second row, α is some constant of order 1, determined by the source the frequency spread. **b** The form of $g^{(1)}(\tau)$ for partially coherent light in the case of Gaussian linewidth. The shape of the envelope is given by $\langle e^{i(\phi(t+\tau)-\phi(t))} \rangle$. The peak in the envelope is at $\tau = 0$

perfectly coherent light, $g^{(1)}(\tau) = 1$ is constant, while for perfectly incoherent light the correlation function is a Dirac delta function, $g^{(1)}(\tau) = \delta(\tau)$. These are shown in Fig. 2.2a

Light that falls between these two extremes and has a finite coherence time is called *partially coherent*. Light produced by a thermal source is partially coherent. If the light source is a hot gas, collisions between molecules and random Doppler shifts broaden the lines to give a spread of frequencies and therefore a finite width to $g^{(1)}(\tau)$. Such thermally generated partially coherent light is often referred to as *chaotic light*. Two models are generally used to describe the thermal line broadening, in which the averaged term in Eq. (2.8) is either Gaussian or Lorentzian.

In the Gaussian case, where the frequency spread is primarily dominated by inhomogeneous processes like Doppler broadening, the temporal correlation function is

$$g^{(1)}(\tau) = e^{-i\omega\tau} e^{-\frac{\pi}{2}\left(\frac{\tau}{\tau_c}\right)^2}, \tag{2.9}$$

where $\tau_c = \frac{\sqrt{8\pi \ln 2}}{\Delta\omega}$. In the Lorentzian case, due to homogeneous processes like collisional broadening or the natural broadening of an excited state due to its finite lifetime, we instead have

$$g^{(1)}(\tau) = e^{-i\omega\tau} e^{-|\tau|/\tau_c}, \tag{2.10}$$

with coherence time $\tau_c = \frac{1}{\Delta\omega}$.

Given an amplitude interference pattern, the interference visibility is defined by

$$\mathcal{V} = \frac{I_{\max} - I_{\min}}{I_{\max} + I_{\min}}, \tag{2.11}$$

where $I_{\max}$ and $I_{\min}$ are the maximum and minimum intensities (see Fig. 2.3). One of the reasons that the temporal correlation function is important is that it is directly related to interference visibility. Imagine two fields $E_1(t)$ and $E_2(t+\tau)$ interfering, where τ is the additional time one wave propagated relative to the other in order to reach the point at which interference is considered. Then the total amplitude is $E(t) = E_1(t) + E_2(t+\tau)$, and the intensity averaged over a short time interval is

$$\begin{aligned}
\langle I \rangle &= \langle \hat{E}_1^{(-)}(t)\hat{E}_1^{(+)}(t)\rangle + \langle \hat{E}_2^{(-)}(t+\tau)\hat{E}_2^{(+)}(t+\tau)\rangle + 2\,\mathrm{Re}\langle \hat{E}_1^{(-)}(t)\hat{E}_2^{(+)}(t+\tau)\rangle \\
&= \langle I_1\rangle + \langle I_2\rangle + 2\,\mathrm{Re}\langle \hat{E}_1^{(-)}(t)\hat{E}_2^{(+)}(t+\tau)\rangle \qquad (2.12) \\
&= \sqrt{\langle I_1\rangle\langle I_2\rangle}\left[\sqrt{\frac{\langle I_1\rangle}{\langle I_2\rangle}} + \sqrt{\frac{\langle I_2\rangle}{\langle I_1\rangle}} + \mathrm{Re}\left(\frac{\langle \hat{E}_1^{(-)}(t)\hat{E}_2^{(+)}(t+\tau)\rangle}{\sqrt{\langle I_1\rangle\langle I_2\rangle}}\right)\right] \qquad (2.13) \\
&= \sqrt{\langle I_1\rangle\langle I_2\rangle}\left[\sqrt{\frac{\langle I_1\rangle}{\langle I_2\rangle}} + \sqrt{\frac{\langle I_2\rangle}{\langle I_1\rangle}} + \mathrm{Re}\left(g^{(1)}(\tau)\right)\right]. \qquad (2.14)
\end{aligned}$$

The first two terms in the brackets are constants, and the third term contains the oscillations. Since $-|g^{(1)}(\tau)| \le \mathrm{Re}\left(g^{(1)}(\tau)\right) \le +|g^{(1)}(\tau)|$, it is found that

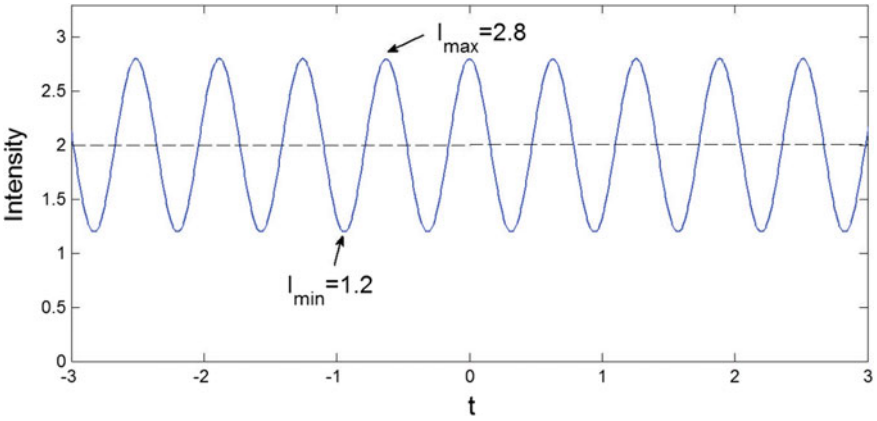

Fig. 2.3 An interference pattern with mean intensity $I = 2$ and visibility $\mathcal{V} = \frac{I_{\max}-I_{\min}}{I_{\max}+I_{\min}} = \frac{2.8-1.2}{2.8+1.2} = 0.4$, in units where the intensity is dimensionless

$$\mathcal{V} = |g^{(1)}(\tau)|. \tag{2.15}$$

Spatial correlations may also be considered. Setting the two times equal, but looking at two different spatial points, the spatial correlation function is

$$g_s^{(1)}(\Delta r) = \frac{G^{(1)}(\boldsymbol{r}, \boldsymbol{r}+\Delta\boldsymbol{r}; t, t)}{G^{(1)}(\boldsymbol{r}, \boldsymbol{r}; t, t)}, \tag{2.16}$$

where stationary fields have again been assumed. The correlations should decay as the transverse distances (perpendicular to the propagation direction) become large, so that one may define a *transverse coherence length* d_c as the transverse distance at which decay sets in. d_c is sometimes defined as the square root of the *coherence area*, $d_c = \sqrt{A_c}$. A_c is defined to be the size of the area around one point in the wave, perpendicular to the propagation direction, in which other points have a stable enough phase relation with the first point to create interference. Then, similarly to the temporal case, a system may be described as spatially coherent or spatially incoherent if its size is, respectively, much less than or much greater than d_c. A second coherence length can also be defined, the *longitudinal coherence length*, l_c, which is the spatial distance covered by the light during one coherence time unit: $l_c = c\tau_c$.

Because the coherence time tends to be very short for true thermal light (blackbody radiation), which often has $\tau_c < 10^{-9}$ s, in experiments *pseudothermal* light may be used instead. This is produced by scattering coherent light from a rotating ground glass surface. Light scattering from different points in the surface travel different distances, so that spatially and temporally random patterns of constructive and destructive interference occur if the light is shown onto a screen. These patterns are called *speckles*, and they vary randomly over time as the glass disk rotates.

For light from a TM_{00} laser mode striking the disk at distance r from the axis, the coherence time of these speckles is given by the formula

$$\tau_c = \frac{w_0}{2\sqrt{\pi} r \Omega}, \tag{2.17}$$

where w_0 is the beam diameter at the disk and Ω is the rotational frequency of the disk. In this way, longer coherence times, typically $1\,\mu\text{s} \leq \tau_c \leq 1\,\text{ms}$, can be obtained. If the light strikes a screen at distance z from the disk, a typical speckle size is of order $d = \frac{\lambda z}{2w_0}$.

2.2.2 Second-Order Correlations

In the next section, and in later chapters, it is often useful to consider the correlation between two intensities, rather than between two fields. The corresponding correlation function is called the (normalized) *second-order correlation function* [3], $g^{(2)}(\tau)$. Similarly to the first-order case, we may look at both spatial and temporal correlations, but here we restrict ourselves to the temporal case. Suppressing the spatial variables again, the correlation is defined by

$$g^{(2)}(\tau) = \frac{\langle \hat{I}(t)\hat{I}(t+\tau)\rangle}{\langle \hat{I}(t)\rangle\langle \hat{I}(t+\tau)\rangle} = \frac{\langle \hat{I}(t)\hat{I}(t+\tau)\rangle}{\langle \hat{I}\rangle^2}, \tag{2.18}$$

where in the second equality the average intensity has been assumed to be time-independent. Using the fact that the intensity is the absolute square of the field, one may also write

$$g^{(2)}(\tau) = \frac{\langle \hat{E}^{(-)}(t)\hat{E}^{(-)}(t+\tau)\hat{E}^{(+)}(t)\hat{E}^{(+)}(t+\tau)\rangle}{\langle \hat{E}^{(-)}(t)\hat{E}^{(+)}(t)\rangle^2}, \tag{2.19}$$

or, since the intensity is proportional to the number of photons, $g^{(2)}$ may alternatively be written in the form

$$g^{(2)}(\tau) = \frac{\langle \hat{N}(t)\hat{N}(t+\tau)\rangle}{\left(\langle \hat{N}(t)\rangle\right)^2}, \tag{2.20}$$

where $\hat{N} = \hat{a}^\dagger\hat{a}$ is the photon number operator.

For perfectly coherent monochromatic light, $g^{(2)}(\tau) = g^{(2)}(0) = 1$ is constant. For classical light, $g^{(2)}(\tau)$ is largest at $\tau = 0$ and decays monotonically with increasing τ, just as for the first-order correlation function. However, for anti-bunched, non-classical states of light (see below), $g^{(2)}(\tau)$ exhibits unusual behavior and actually grows for nonzero τ, $g^{(2)}(\tau) > g^{(2)}(0)$.

For partially coherent thermal light, where light scatters multiple times before exiting the source, the first and second-order correlations functions are connected by Siegert's relation

$$g^{(2)}(\tau) = 1 + |g^{(1)}(\tau)|^2. \tag{2.21}$$

Since $g^{(1)}(\tau)$ decays from 1 at short times to 0 at long times (much greater than τ_c), it follows that $g^{(2)}(\tau)$ decays from $g^{(2)}(0) = 2$ to $g^{(2)}(\infty) = 1$. For the Lorentzian and Gaussian cases, the Siegert relation implies that:

$$g^{(2)}(\tau) = 1 + e^{-2|\tau|/\tau_c} \qquad \text{(Lorentzian)} \tag{2.22}$$

$$g^{(2)}(\tau) = 1 + e^{-\pi(\tau/\tau_c)^2} \qquad \text{(Gaussian)}, \tag{2.23}$$

for thermal light.

The intensity can always be written as a mean value plus some randomly fluctuating term, $I(t) = \langle I \rangle + \Delta I(t)$. Regardless of the source of the fluctuations, ΔI, they must have vanishing mean, $\langle \Delta I \rangle = 0$, so if it is assumed that the average intensity is time independent then the second-order coherence function can be written as

$$\begin{aligned} g^{(2)}(\tau) &= \frac{\langle (\langle I \rangle + \Delta I(t))\,(\langle I \rangle + \Delta I(t+\tau)) \rangle}{\langle I \rangle^2} \\ &= 1 + \frac{\langle \Delta I(t) \Delta I(t+\tau) \rangle}{\langle I \rangle^2}. \end{aligned} \tag{2.24}$$

Therefore, $g^{(2)}(\tau)$ can be seen as a measure of the correlation between the intensity *fluctuations* at different times. Equivalently, since the intensity is proportional to the number of photons present, it measures correlations between photon number fluctuations.

Looking at the case of zero time delay, $\tau = 0$, three possibilities can be distinguished. (i) If $g^{(2)}(0) = 1$, then the distribution of times between photon emissions are given by a Poisson distribution. This is the case for light in a coherent state. (ii) If $g^{(2)}(0) > 1$, then the spacings between photons are reduced from the Poisson case. In other words, the photons tend to cluster together more than in the Poisson case. This case is called *super-Poisson*, and the light is often referred to as *chaotic* or *photon-bunched*. Thermal light sources produce photon-bunching. (iii) If $g^{(2)}(0) < 1$, then the spacings between photons are increased. This is called *sub-Poisson* or *anti-bunched* light.

Both the Poisson and super-Poisson cases are possible classically, however the sub-Poisson case is not. So the appearance of sub-Poisson or anti-bunched light is a clear signal of non-classical behavior.

First-order correlation functions are measured by comparing the output of a single detector at different locations or times, while second-order correlation functions are measured by detecting two photons in two separate detectors. In a similar manner, higher nth-order correlation functions can be defined and can be measured using n-detector arrangements. These have been used, for example, to study higher-order ghost imaging [4–9].

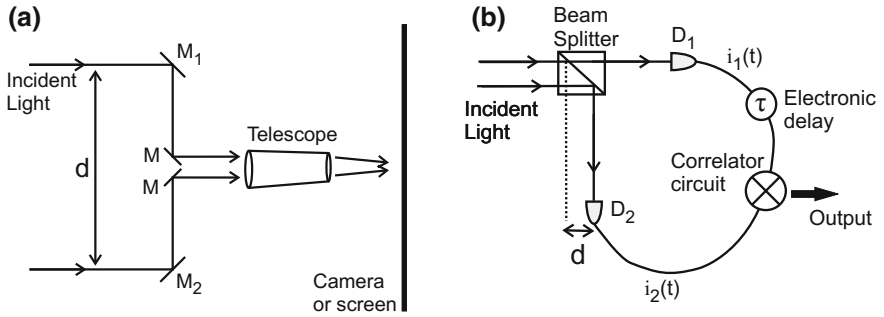

Fig. 2.4 Two stellar interferometers. **a** The Michelson stellar interferometer, in which coherence between field amplitudes at points separated by distance d is measured. Mirrors M_1 and M_2 reflect light from different points in the wavefront into a telescope, where they are focused to produce an interference pattern, **b** the Hanbury Brown and Twiss interferometer. In this apparatus, *intensities* rather than merely simple amplitudes are correlated at points separated by d. Two photodetectors send photo currents i_1 and i_2 to an electronic circuit that correlates the signals. The output signal is the mean product of currents, $\langle i_1(t) i_2(t+\tau)\rangle$, which is proportional to the mean product of intensities, $\langle I_1(t) I_2(t+\tau)\rangle$. In the case of low photon numbers, the electronic correlator becomes a photon coincidence counter

2.3 Hanbury Brown and Twiss: Source Size from Correlation

Classical interference theory is built around first-order (field or amplitude) correlations. The importance of second-order (intensity or photon number) correlations first became clear through the work of Hanbury Brown and Twiss (HBT) on stellar diameter measurements in the 1950s.

Prior to the work of HBT, the principal means of measuring stellar diameters was through measurement of spatial coherence via the field correlations measured by $g^{(1)}$. In the Michelson stellar interferometer (Fig. 2.4a) light arriving from a star strikes two mirrors separated by distance d, and then the two reflected beams are combined and sent through a telescope, finally forming an interference pattern in a camera. Light arriving at different angles have maxima and minima shifted in position by a distance proportional to the angle. So, if the angular size of the star is too large, all of the shifted fringes from different angular directions end up washing out the interference pattern. The pattern is lost when the angular spread $\delta\theta_S$ of the starlight is smaller than the angular resolution $\Delta\theta_I$ of the interferometer. The spread $\delta\theta_S$ is determined by the size of the star and its distance L from earth, $\delta\theta_S = \frac{D}{L}$, for $L \gg D$. The angular resolution, on the other hand, is determined by the wavelength used and by the size of the interferometer, $\Delta\theta_I = \frac{1.22\lambda}{d}$, where the factor of 1.22 comes from the width of the Bessel function determining the resolution of the circular telescope aperture, as in Eq. A.32 of "Appendix A." The requirement that $\delta\theta_S < \Delta\theta_I$ then places a limit on how large d can be before the interference is lost, since we must have

$$\frac{D}{L} < \frac{1.22\lambda}{d}. \tag{2.25}$$

By varying d and finding the distance $d = l_c$ at which the pattern is lost, we then have an estimate for the stellar diameter, $D = 1.22\lambda\frac{L}{l_c}$. l_c is then the transverse spatial coherence length of the light.

Such field interference methods provide a great improvement in angular resolution over other methods, since the distance d can be made much larger than the diameter of the telescope. However, it has several drawbacks: (i) the ability to collect light is lower, so that dim objects can not be effectively measured, (ii) the measurement is susceptible to atmospheric turbulence, and (iii) a high level of mechanical stability must be maintained in the distances between the mirrors and the telescope, which becomes increasingly difficult as d becomes larger.

The HBT approach can be seen as replacing the two mirrors of the Michelson interferometer by two independent photodetectors, D_1 and D_2, separated by distance d (Fig. 2.4b). The detectors produce two photocurrents proportional to the incident light intensities at those points. After a time delay τ is imposed on one current, the two signals are then fed into an electronic circuit that multiplies the currents and integrates over an interval of time in order to produce an average. The net result is proportional to the expectation value $\langle I_1(t)I_2(t+\tau)\rangle = \langle I(r_1,t)I(r_1+d,t+\tau)\rangle$, where I_1 is the intensity in detector D_1 (located at r_1), and I_2 is the intensity at D_2 (located at $r_2 = r_1 + d$). From this, the second-order correlation function $g^{(2)}(d,\tau)$ may be found. By setting $\tau = 0$ and varying the distance d between the detectors, the coherence length l_c can be determined. Alternatively, the distance can be fixed and the time delay may be varied in order to find the coherence time.

2.4 From One-Photon to Two-Photon Interference

Yet another important interferometer, which appears in multiple guises in this book, is the Mach–Zehnder interferometer, shown in basic form in Fig. 2.5. It was discussed in the previous chapter, where it was considered as a means of producing spatial-mode qubits. Here, it is treated in more detail. There are two input ports, 1 and 2 on the left, and two output ports, 3 and 4, on the right. Suppose light enters through one input, say port 1, and optical detectors are placed at the outputs. Assume also that the input light is perfectly coherent. Then, the first beam splitter sends the light either along the upper path or the lower path, with equal probability. A phase shift ϕ can be introduced to the portion of the light following the upper path, for example, by changing the path length or by introducing a small piece of glass of refractive index $n \neq 1$ into the light's path. The two beams recombine at the second beam splitter, now possibly out of phase with each other, leading to constructive or destructive interference as ϕ is varied. Let the input and output states of the light be described by the two-component vectors

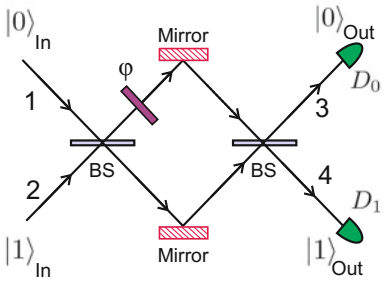

Fig. 2.5 The Mach–Zehnder interferometer. Light input at one port (1 or 2) has two possible paths through the system before leaving at another port (3 or 4). Depending on the phase shift introduced into one path, the output can be steered in one direction or the other, analogous to the *bright* and *dark spots* the Young experiment

$$|\psi_{in}\rangle = \begin{pmatrix} \psi_1 \\ \psi_2 \end{pmatrix}, \quad |\psi_{out}\rangle = \begin{pmatrix} \psi_3 \\ \psi_4 \end{pmatrix}, \tag{2.26}$$

where ψ_n is the amplitude at port n. The "amplitude" here can be either the classical electric field in the case of bright light, or the quantum mechanical amplitude in the case of single-photon input. The action of each beam splitter can be represented as a matrix $M_{\rm BS}$ ("Appendix A") and the phase shift by matrix M_ϕ, where

$$M_{\rm BS} = \begin{pmatrix} 1 & i \\ i & 1 \end{pmatrix}, \quad M_\phi = \begin{pmatrix} e^{i\phi} & 0 \\ 0 & 1 \end{pmatrix}, \tag{2.27}$$

so that

$$|\psi_{out}\rangle = M_{\rm BS} M_\phi M_{\rm BS} |\psi_{in}\rangle = \begin{pmatrix} e^{i\phi} - 1 & i\left(e^{i\phi} + 1\right) \\ i\left(e^{i\phi} + 1\right) & 1 - e^{i\phi} \end{pmatrix} |\psi_{in}\rangle. \tag{2.28}$$

Here, we have ignored the propagation phases $e^{-i\omega t + i\boldsymbol{k}\cdot\boldsymbol{x}}$ and mirror reflection phases that are common to all terms. So if the light is all incident on port 1 ($\psi_2 = 0$), we find that the output at port 3 is $\psi_3 = e^{i\phi} - 1$. The resulting intensity (in the bright light case) or detection probability (in the single photon case) is, therefore, proportional to $|\psi_{out}|^2 = |\psi_3|^2 = |e^{i\phi} - 1|^2 = 2\,(1 - \cos\phi)$.

However, instead of looking at the output of each detector separately, one may follow the lead of Hanbury Brown and Twiss, by looking at joint detections in the pair of detectors. In other words, coincidence counts are measured, providing measurement of the second-order correlation function. The interference is now between two-photon amplitudes, instead of single-photon amplitudes. The coincidence counting is done by using an electronic gate which only registers a count if there is a signal coming in from both detectors within some very short time window.

It can be shown that there is a complementarity between the single-photon and double-photon visibilities, $\mathcal{V}_1$ and $\mathcal{V}_{12}$ in any system [10, 11]. In particular, $\mathcal{V}_1^2 + \mathcal{V}_{12}^2 \leq$

1, or equivalently, $\mathcal{V}_1\mathcal{V}_{12} \leq \frac{1}{2}$. Thus to achieve strong two-photon interference, it is necessary to make the observation of single-photon effects unobservable. (See the Franson interferometer, Sect. 2.6, for an example of this.)

2.5 The Hong–Ou–Mandel Dip

The *Hong–Ou–Mandel (HOM) dip* [12] is an interference effect that occurs in the coincidence rate of two-photon interferometers. Besides opening a new arena for the exploration of quantum mechanical two-photon interference effects, the HOM dip has shown itself useful in measuring extremely short (sub-femtosecond) time intervals. It is also used to reconstruct the temporal profile of single photon wave packets [12], to measure the delay times caused by passage of light through materials [13], and to make measurements of tunneling times of single photons through barriers [14]. Of particular importance here is the fact that if a dispersive material is placed in one of the possible photon paths of the interferometer used to observe the dip, the effect of group velocity dispersion (GVD) cancels from the coincidence rate. In other words, there is no dispersive broadening of wave packets. This effect is discussed in more detail in Chap. 3.

Figure 2.6 shows the *HOM interferometer*. The signal and idler from parametric down conversion take separate paths to a 50/50 beam splitter, with a variable delay inserted into one of the paths, before the beam splitter. The signal takes path a to the beam splitter and the idler takes path b. After the beam splitter, the outgoing photons reach two detectors, where the coincidence count is recorded. As the delay time is scanned, the coincidence rate traces out a roughly triangular dip, as shown in Fig. 2.7. Ideally, the dip reaches a minimum of zero (100 % visibility) when the delay vanishes. It is essential that the indistinguishability of the two photons be maintained for this effect to appear. Any factors that increase the ability to distinguish which path was taken by which photon after the beam splitter causes a corresponding decrease in the visibility of the dip. When the translatable mirror is moved a distance δl, a delay of $\delta\tau = \delta l/c$ is introduced between the two paths, along with a phase difference of $\delta\phi = \delta l/\lambda$.

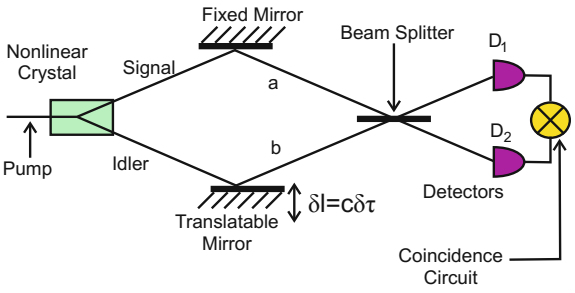

Fig. 2.6 The Hong–Ou–Mandel (HOM) interferometer. The translatable mirror introduces a phase shift between the signal and idler, which are then mixed at the beam splitter before coincidence detection

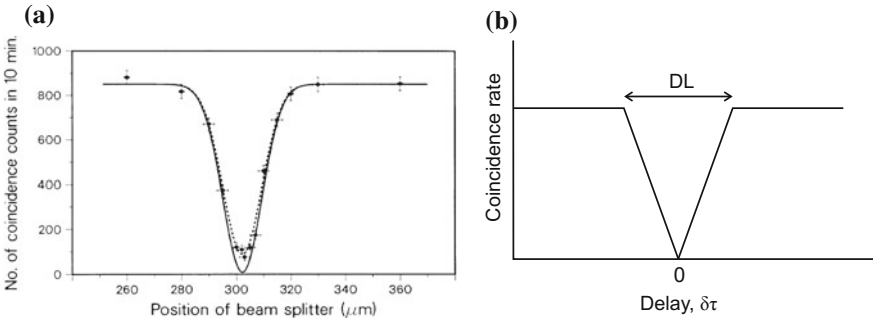

Fig. 2.7 The HOM dip. The coincidence rate exhibits a *triangular* dip, vanishing at zero time delay. **a** Experimental data showing the dip arising from interference of signal and idler [12], **b** idealized dip arising from interference of two square amplitudes

The explanation for the HOM dip is very simple. Assume for a moment that there is no delay. In order for a coincidence count to be registered, exactly one of the photons must reach each of the two detectors. This can happen in one of two ways: either both photons are reflected at the beam splitter (RR) or both are transmitted (TT). Because each reflection at the beam splitter introduces a phase shift of $\pi/2$, the amplitudes for these two possibilities have opposite sign. In the case of a symmetric 50/50 beam splitter (reflectance = transmittance = 50 %), the RR and TT amplitudes are also equal in magnitude, so that they exactly cancel, giving a vanishing coincidence rate. Now, if a delay is introduced, this allows the photons to be distinguished by their arrival times. The interference is reduced and the cancelation becomes only partial. As the delay increases from zero, the coincidence rate rises from zero back to the classically expected value.

Quantitatively, the coincidence rate is given by

$$R_c(\delta\tau) = R_0 \left\{ 1 - \frac{1}{4} \frac{\int g^*(\tau) g(2\,\delta\tau - \tau) d\tau}{\int |g(\tau)|^2 d\tau} \right\}, \tag{2.29}$$

where R_0 is a constant, $g(\tau) = \frac{G(\tau)}{G(0)}$, and $G(\tau)$ is the Fourier transform of the spectral function $\Phi(\omega)$. Assuming a Gaussian pump and using the function $\Phi(\omega) = sinc\,(\omega T)$ for SPDC (see Chap. 1), the coincidence rate is

$$R_c(\delta\tau) = R_0 \left(1 - e^{-\Delta\omega^2 \delta\tau^2} \right), \tag{2.30}$$

for some constant R_0 [12]. Here, $T \sim \frac{1}{\Delta\omega}$ is the width of the photon wavepacket. The experimental data for the coincidence rate matches this expression well, as seen in Fig. 2.7a.

To give an idea of why the coincidence rate has this form, imagine a simplified situation in which the spectrum is flat, and where the signal and idler amplitudes

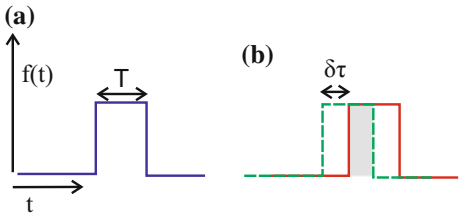

Fig. 2.8 Two *rectangular* amplitudes of unit height and of width T (**a**), have an overlap given as by Eq. (2.32) when one is displaced by time $\delta\tau$ relative to the other (**b**)

both have unit-height rectangular shapes (Fig. 2.8a) of the form

$$f(t) = \begin{cases} 1, & \text{for } |t| \leq \frac{T}{2} \\ 0 & \text{for } |t| > \frac{T}{2}, \end{cases} \tag{2.31}$$

where T is the time for the photons to cross the nonlinear crystal. This is a reasonable first approximation, since the amplitude for pair creation drops suddenly to zero at the edge of the crystal. Suppose that one photon is delayed relative to the other by delay time $\delta\tau$. Then, the overlap of these amplitudes is given by the convolution

$$I(t) = \int_{-\infty}^{\infty} f(t) f(t - \delta\tau) dt \; = \; \begin{cases} 1 - \frac{|\delta\tau|}{T}, & \text{for } |t| \leq T \\ 0 & \text{for } |t| > T. \end{cases} \tag{2.32}$$

Examining Fig. 2.8b, the reader can verify that this expression is simply the area of overlap between the two shifted square functions. This overlap is triangular, having maximum value at $\delta\tau = 0$ and decaying linearly to zero with increasing $|\delta\tau|$, representing constructive interference between the amplitudes. In the case of destructive interference, this triangular overlap is subtracted from the constant noninterfering value of 1, so that

$$R_c(\delta\tau) = R_0 \left\{ 1 - \frac{1}{2} \Lambda \left(\frac{2\delta\tau}{T} \right) \right\}, \tag{2.33}$$

where

$$\Lambda(x) = \begin{cases} 1 - |x|, & \text{for } |x| \leq 1 \\ 0, & \text{for } |x| > 1 \end{cases} \tag{2.34}$$

is the triangle function. The idealized form of Eq. (2.33) provides a good approximation to Eq. (2.30). This ideal coincidence rate is plotted in Fig. 2.7b. The experimental data of Fig. 2.7a roughly matches this and gives a generally triangular shape, but more rounded because the photon creation amplitudes in reality are sinc functions, rather than squares.

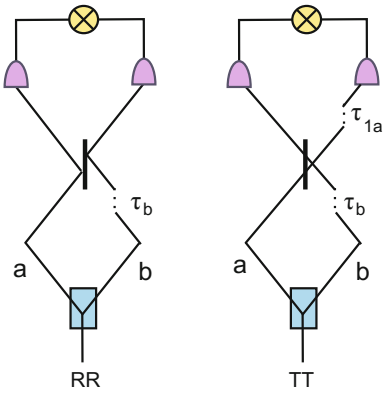

Fig. 2.9 Signal and idler need not overlap temporally on the beam splitter to interfere and produce an HOM dip. Here, τ_a is a time delay that effects only the signal photon in branch a. If $\tau_a = 2\tau_b$, then both the RR and TT cases lead to the same time delay $\Delta t \equiv t_2 - t_1 = \tau_b$ between detection of photons. The two outcomes are therefore indistinguishable and can interfere

2.6 The Franson Interferometer

As was the case in the discussion of single-photon interference, it must be borne in mind that "two-photon" interference is not the result of one photon interfering with a second photon; more generally, it is the interference of one potential two-photon state with another potential state of the same two-photon system. The two photons involved need not arrive at a beam splitter at the same time or ever meet at all for interference to occur. Only indistinguishability, not temporal overlap, is required. This was demonstrated by the experiment of [15], where a fixed delay was introduced in one path before the beam splitter, so that the two photons arrived at the beam splitter well separated in time (Fig. 2.9). In order to restore distinguishability, postponed compensation was used; i.e. a selective time delay was added after the beam splitter that only affects the polarization traveling in branch a. The RR (reflection/reflection) and TT (transmission/transmission) cases may then be pictured as in Fig. 2.9. In the RR case the idler arrives at detector 2, delayed by a time τ_b, so that the time difference between the two detections is $\Delta t \equiv t_2 - t_1 = \tau_b$. However, in the TT case the signal arrives at detector 2, delayed by τ_{1a}, while the idler arrives at detector 1 delayed by τ_b. Thus, in this case, the detection time difference is $\Delta t \equiv t_2 - t_1 = \tau_a - \tau_b$. So, if delays are chosen such that $\tau_a = 2\tau_b$, both cases have the same time difference, $\Delta t = \tau_b$. Since the time difference is the same for the RR and TT possibilities, they cannot be distinguished and the interference dip appears, even though the two photons never overlap on the beam splitter. This apparent nonlocality of the interference again demonstrates that the HOM dip is a purely quantum effect.

A similar effect can be seen in the Franson interferometer [16] shown in Fig. 2.10. The nonlinear crystal at the left is pumped by a beam at frequency ω_p. Each photon from a down conversion pair enters a separate path. Each of those photons then has

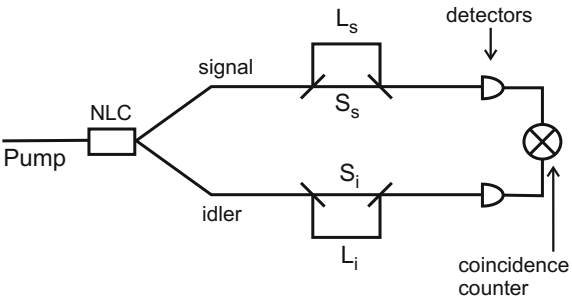

Fig. 2.10 The Franson interferometer. Each photon can travel via a long path or a short path. After post-selection to remove long-short interference, the amplitude for both to follow the long path interferes with the amplitude for both following the short path

a choice of two possible subpaths, one long and one short. At the other end, the two photons are then detected in coincidence. The difference of path lengths between the long and short paths is much longer than the photon coherence time, so that there no single-photon interference occurs between the long and short paths.

Since the time at which the pair is created is unknown, the cases where both photons take the long path (LL) and where both take the short path (SS) are indistinguishable, and so these two-photon states should interfere with each other. The visibility of this interference can be greatly enhanced by post-selection: take the coincidence window short enough to reject the two cases L_1S_2 and S_1L_2 in which one photon takes the long path and one takes the short path. In this case, the two-photon visibility is ideally 100 %, despite the fact that the two photons are never in the same location and so have no opportunity to interfere in the sense of classical waves.

Let Δl_s and Δl_i be the path difference between the long and short paths for the signal and idler respectively. Then, the phase difference between the LL path and the SS path is

$$\phi = \frac{\omega_\mathrm{s}\Delta l_\mathrm{s}}{c} + \frac{\omega_\mathrm{i}\Delta l_\mathrm{i}}{c} \approx \frac{1}{2}\omega_\mathrm{p}\left(\Delta l_\mathrm{i} + \Delta l_\mathrm{s}\right), \tag{2.35}$$

so long as $|\omega_\mathrm{s} - \omega_\mathrm{i}|$ is small compared to the central frequency $\omega_0 = \frac{\omega_\mathrm{p}}{2}$. The coincidence probability is

$$P_c = |\langle\psi|\psi\rangle|^2 = \frac{1}{4}|1 + e^{i\phi}|^2 \tag{2.36}$$

$$= \frac{1}{2}\left(1 + \cos\phi\right) = \frac{1}{2}\left[1 + \cos\left(\frac{\omega_\mathrm{p}}{2}\left(\Delta l_\mathrm{s} + \Delta l_\mathrm{s}\right)\right)\right]. \tag{2.37}$$

This interference was demonstrated experimentally in [17–20]. The 100 % interference visibility as the path lengths are varied is again an indication of an intrinsically quantum mechanical effect.

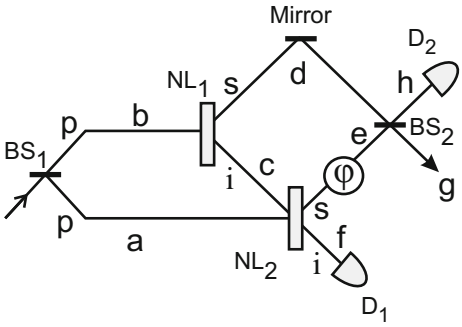

Fig. 2.11 Schematic of setup for two-crystal interference experiment. The pump can undergo down conversion in either of two crystals. If the two signal modes and the two idler modes are sufficiently well overlapped, it is impossible to tell in which crystal the down conversion occurred. In that case, the amplitudes for both possibilities overlap and first-order interference can occur between the two potential signal photons at detector D_2. In the figure, p, s, and i stand, respectively, for pump, signal, and idler, and *a–h* label points in the possible photon paths

2.7 Double-Crystal Experiments and Induced Coherence

The existence of interference between two amplitudes requires that it is impossible to tell which amplitude was actualized; in particular, an interferometer only exhibits interference when it is impossible in principle for one to tell which path the photons took through the arrangement. As the degree of path distinguishability increases, the visibility of the interference pattern goes down. In addition, there is often a form of complementarity between single-photon (field or amplitude) interference and two-photon (intensity) interference [10, 11]: in most experiments, as the visibility of one type of interference goes up, the other goes down.

A highly counter-intuitive experiment that can exhibit first and second order interference simultaneously uses the Zhou–Wang–Mandel two-crystal interferometer shown schematically in Fig. 2.11 [21–23]. A pump beam is passed through a 50/50 beam splitter, so that each photon has equal amplitude to enter either of two nonlinear crystals, NL_1 or NL_2. Imagine that a pump photon undergoes down conversion in one of the crystals. If the two crystals are very well aligned, so that the paths of the idlers produced by the crystals completely overlap, then it is impossible to tell whether an idler photon detected at detector D_1 came from the second crystal or the first one. Similarly, it is impossible to detect which crystal produced a signal photon detected at D_2. Because it is impossible to distinguish whether the down conversion occurred in NL_1 or NL_2, the amplitudes for both possibilities must be added. By varying the phase shift introduced between the two potential signal paths, interference is then seen at D_2.

However, if the idler path between NL_1 and NL_2 is blocked at point c, then any idler arriving at D_1 must have come from NL_2. It is found that the interference at D_2 then disappears, since the presence or absence of an idler detection at D_2

gives information about which crystal the pair was born in. The presence of this path information makes the two amplitudes distinguishable. The interesting (or even "mind-boggling" [24]) thing is that only the *idler* photons are blocked by the filter at c, yet the interference pattern in the *signal* at D_2 disappears, despite the fact that the signal never passed through c. If a beam splitter is placed at c, it is found that the visibility of the interference is decreased in proportion to the reflectance of the beam splitter; the more reflective the beam splitter, the more path information can be obtained by monitoring the presence of idler photons at D_1 (or alternatively, by monitoring those reflected at c). Note that these photons do not actually have to be detected in order for the interference visibility to be affected. The simple *possibility* of their detection is all that is needed to damage the interference.

Second-order interference in the two-detector coincidence counting is to be expected in this setup, between potential biphoton states created in the two different crystals. But the single-photon, first-order interference occurring at a single detector may seem surprising. Because there is no fixed phase relation between the signal and idler photons, there can be no first-order interference effects between them. However, there can be single-photon interference between the two amplitudes for signal photons arising in the two different crystals due to the same pump. The phase of the full biphoton state is determined by the phase of the pump beam [25], so that different potential histories of the signal photons created in the different crystals should be capable of interfering with each other, even though the signal by itself is of low coherence. This hidden information about the pump phase that is retained by the outgoing state has been referred to as a *phase memory effect*. The single-photon and biphoton interferences show up, respectively, in the first and second-order correlation functions $g^{(1)}(\tau)$ and $g^{(2)}(\tau)$.

If the pump intensity is low enough so that the probability of the idler from one crystal inducing down conversion in the other is negligible, the single-photon interference becomes noticeable, since the experimental arrangement cannot distinguish between down conversion photons produced at one crystal and those produced at the other. In this case, if point c is unblocked, D_1 fires every time D_2 fires (assuming perfect detectors and no photon losses). While indistinguishability is maintained, the potential idler photons originating in the two crystals are mutually coherent, as are the two signals; this is referred to as *induced coherence* between the crystals. There should then be first-order interference between the two possible signal photons. The coherence is induced by the act of matching the modes of the two idlers to maintain indistinguishability.

It has been shown [26–28] that interference can be obtained by varying the phase between the two signals, or by varying the relative phase of the two pump beams after BS_1. In both cases, interference arises in *both* the singles ($g^{(1)}(\tau)$) and coincidence ($g^{(2)}(\tau)$) counting rates. When varying signal phase, the interference has a fringe period corresponding to the frequency of the signal photons. In contrast, if the pump phase is varied, the coincidence rate and signal count rate both have fringes with the period expected from the pump frequency.

For a more quantitative discussion of the interferometer, note that after BS_1 the state is

$$\frac{1}{\sqrt{2}}\left(i|1\rangle_a|0\rangle_b + |0\rangle_a|1\rangle_b\right). \tag{2.38}$$

After crystal NL_1, the pump photon at b undergoes down-conversion so that the state becomes

$$\frac{1}{\sqrt{2}}\left(i|1\rangle_a|0\rangle_c|0\rangle_d + |0\rangle_a|1\rangle_c|1\rangle_d\right). \tag{2.39}$$

Following the second crystal, NL_2, and the phase shift, the state becomes:

$$\frac{1}{\sqrt{2}}\left(ie^{i\phi}|0\rangle_c|0\rangle_d|1\rangle_e|1\rangle_f + |1\rangle_c|1\rangle_d|0\rangle_e|0\rangle_f\right). \tag{2.40}$$

But the idler at c continues through NL_2 to appear at f, so that if the two idlers are indistinguishable, this becomes

$$\frac{1}{\sqrt{2}}\left(ie^{i\phi}|0\rangle_d|1\rangle_e + |1\rangle_d|0\rangle_e\right)|1\rangle_f. \tag{2.41}$$

After the final beam splitter, the result is

$$\frac{1}{2}\left[ie^{i\phi}\left(|0\rangle_g|1\rangle_h + i|1\rangle_g|0\rangle_h\right) + \left(|1\rangle_g|0\rangle_h + i|0\rangle_g|1\rangle_h\right)\right]|1\rangle_f \tag{2.42}$$

$$= \frac{1}{2}\left[i\left(e^{i\phi}+1\right)|0\rangle_g|1\rangle_h - \left(e^{i\phi}-1\right)|1\rangle_g|0\rangle_h\right]|1\rangle_f. \tag{2.43}$$

The probability of detection at D_1 (point h) is thus

$$\frac{1}{4}\left|e^{i\phi}+1\right|^2 = \frac{1}{2}\left(1+\cos\phi\right), \tag{2.44}$$

exhibiting interference with (ideally) 100 % visibility. If a filter of transmissivity t is placed at point c, this becomes

$$\frac{1}{2}\left(1 + t\ \cos\phi\right). \tag{2.45}$$

It is clear that the interference visibility is proportional to t and that the pattern disappears completely if the idler path at c is blocked ($t \to 0$). This is because if c is blocked then the path can be determined by checking for idler photons at D_1; the existence of this which-path information destroys the interference pattern.

Rather than carrying out an interferometric experiment using the apparatus of Fig. 2.11, it is natural to consider if an object can be imaged with it. Instead of placing a filter of fixed transmissivity t at point c, consider an object with a spatially dependent transmissivity, $T(x, y)$, where x and y are coordinates perpendicular to the propagation axis. Then adding some lenses and beam splitters, the new apparatus

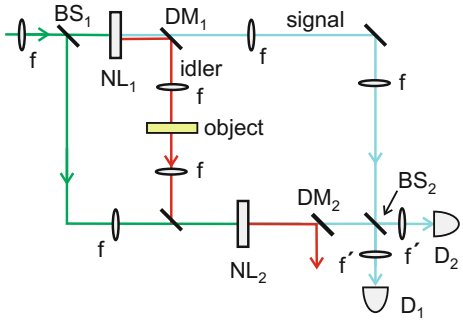

Fig. 2.12 Schematic of setup to produce an image with photons that never saw the object. $DM_{1,2}$ are dichroic mirrors which transmit the signal frequency and reflect the idler frequency. After the second nonlinear crystal, NL_2, DM_2 ejects the idlers from the system. The remaining signal amplitudes mix and are detected at D_1 and D_2

is as shown in Fig. 2.12 [29]. All the lenses are assumed to have the same focal length, f, except possibly the two before the detectors (f'). If a pump photon creates a down conversion pair at the first crystal, the dichroic mirror sends the signal and idler into different paths. The image is "imprinted" onto the idler produced at the first crystal; this idler is then passed through the second crystal, where it is again arranged for idlers from the two crystals to be indistinguishable. A dichroic mirror is used to remove the two idlers from the system, leaving just the signal photons. The last beam splitter mixes these signals so that it is not possible to tell whether a detected photon came from the first crystal via the upper path or from the second crystal via the lower path. By the same method used to transfer the phase information from idler to signal in Fig. 2.11, the image information is now transferred by entanglement to the signal. By tracing the field propagations through the system, then schematically, it is found that the intensities at the two outputs have the structures (dropping all the constants) [30]:

$$I_1 \sim 1 + |t|^2 + 2Re(t) \tag{2.46}$$

$$I_2 \sim 1 + |t|^2 - 2\mathrm{Re}(t). \tag{2.47}$$

Since the transmissivity must obey $|t| \leq 1$, the term linear in t is always greater than or equal to the quadratic term for real t; thus, D_1 gives a positive image and D_2 gives a negative image, as seen in the experiment carried out in [29]. Further, the difference of the two amplitudes has the structure

$$I_1 - I_2 \sim \mathrm{Re}(t), \tag{2.48}$$

giving a higher contrast than either detector alone. The magnification is [30, 31]

$$m = \frac{\lambda_s \ f'}{\lambda_i \ f}, \tag{2.49}$$

where λ_s and λ_i are the signal and idler wavelengths. The strange feature of this arrangement is that only the idler photon ever interacts with the object, but the image arises from measurement of the signal photons; the idlers are discarded without being detected.

The theory of the two-crystal imaging arrangement has been further worked out in [31, 32]. Like many of the initially quantum-based effects discussed in this book, it has been shown [33] that most of its features can be mimicked by a bright-source classical arrangement, with higher signal-to-noise ratio.

References

1. G. Jaeger, *Entanglement, Information, and the Interpretation of Quantum Mechanics* (Springer, Berlin, 2009)
2. D.J. Griffiths, *Introduction to Quantum Mechanics*, 2nd edn. (Pearson Education Ltd., Essex, 2004)
3. M. Fox, *Quantum Optics: An Introduction* (Oxford University Press, Oxford, 2006)
4. Y.F. Bai, S.S. Han, Phys. Rev. A **76**, 043828 (2007)
5. D.Z. Cao, J. Xiong, S.H. Zhang, L.F. Lin, L. Gao, K.G. Wang, Appl. Phys. Lett. **92**, 201102 (2008)
6. Q. Liu, X.H. Chen, K.H. Luo, W. Wu, L.A. Wu, Phys. Rev. A **79**, 053844 (2009)
7. K.W.C. Chan, M.N. O'Sullivan, R.W. Boyd, Opt. Lett. **34**, 3343 (2009)
8. Y. Zhou, J. Simon, J.B. Liu, Y.H. Shih, Phys. Rev. A **81**, 043831 (2010)
9. B. Cao, C. Zhang, Opt. Lett. **35**, 2091 (2010)
10. G. Jaeger, M.A. Horne, A. Shimony, Phys. Rev. A **48**, 1023 (1993)
11. G. Jaeger, A. Shimony, L. Vaidman, Phys. Rev. A **51**, 54 (1995)
12. C.K. Hong, Z.Y. Ou, L. Mandel, Phys. Rev. Lett. **59**, 2044 (1987)
13. A.M. Steinberg, P.G. Kwiat, R.Y. Chiao, Phys. Rev. Lett. **68**, 2421 (1992)
14. A.M. Steinberg, P.G. Kwiat, R.Y. Chiao, Phys. Rev. Lett. **71**, 708 (1993)
15. T.B. Pittman, D.V. Strekalov, M.H. Migdall, M.H. Rubin, A.V. Sergienko, Y.H. Shih, Phys. Rev. Lett. **77**, 1917 (1996)
16. J.D. Franson, Phys. Rev. Lett. **62**, 7205 (1989)
17. Z.Y. Ou, X.Y. Zou, L.J. Wang, L. Mandel, Phys. Rev. Lett. **65**, 321 (1990)
18. J. Brendel, E. Mohler, W. Martienssen, Euro. Phys. Lett. **20**, 575 (1992)
19. Y.H. Shih, A.V. Sergienko, M.H. Rubin, Phys. Rev. A **47**, 1288 (1993)
20. P.G. Kwiat, A.M. Steinberg, R.Y. Chaio, Phys. Rev. Lett. **47**, R2472 (1993)
21. X.Y. Zhou, L.J. Wang, L. Mandel, Phys. Rev. Lett. **67**, 318 (1991)
22. L.J. Wang, X.Y. Zhou, L. Mandel, Phys. Rev. A **44**, 4614 (1991)
23. X.Y. Zou, T.P. Grayson, G.A. Barbosa, L. Mandel, Phys. Rev. A **47**, 2293 (1993)
24. D.M. Greenberger, M.A. Horne, A. Zeilinger, Phys. Today **46**, 22 (1993)
25. P. Grangier, M.J. Potasek, B. Yurke, Phys. Rev. A **38**, 3132 (1988)
26. A. Heuer, S. Raabe, R. Menzel, Phys. Rev. A **90**, 045803 (2014)
27. A. Heuer, R. Menzel, P.W. Milonni, Phys. Rev. Lett. **114**, 053601 (2015)
28. A. Heuer, R. Menzel, P.W. Milonni, Phys. Rev. A **92**, 033834 (2015)
29. G.B. Lemos, V. Borish, G.D. Cole, S. Ramelow, R. Lapkiewicz, A. Zeilinger, Nature **512**, 409 (2014)
30. D.S. Simon, M.H. Horne, unpublished notes (2014)

31. M. Lahiri, R. Lapkiewicz, G.B. Lemos, A. Zeilinger, Phys. Rev. A **92**, 013832 (2015)
32. M. Ghalaii, M. Afsary, S. Alipour, A.T. Rezakhani, arXiv:1509.02031 [quant-ph] (2015)
33. J. Shapiro, D. Venkatraman, F.N.C. Wong, Sci. Rep. **5**, 10329 (2015)

http://www.springer.com/978-3-319-46549-4

Quantum Metrology, Imaging, and Communication
Simon, D.S.; Jaeger, G.; Sergienko, A.V.
2017, XII, 273 p. 105 illus., 68 illus. in color., Hardcover
ISBN: 978-3-319-46549-4